Synthesis of Silver Nanoparticle Based Conductive Inks for Additively Manufactured Electronics

William San-Hsi Hwang

A thesis

submitted in partial fulfillment of the

requirements for the degree of

Master of Science in Materials Science and Engineering

University of Washington

2016

Committee:

Christine Luscombe

Dwayne Arola

Program Authorized to Offer Degree:

Materials Science & Engineering

University of Washington

Abstract

Synthesis of Silver Nanoparticle Based Conductive Inks for Additively Manufactured Electronics

William San-Hsi Hwang

Chair of the Supervisory Committee:
Professor Christine Luscombe
Materials Science & Engineering

Printed electronics is an emerging area of study at the forefront of additive manufacturing technology. Additively manufactured electronic devices have many novel application areas, including three-dimensional microbatteries, electrically small antennas, spanning electrodes and printed circuit boards.[1–3] Conductive features, the backbone of all electronic devices, are typically printed with colloidal solutions of silver nanoparticles. Of the well-studied metallic nanoparticle systems, silver exhibits the highest conductivity and is commonly used in commercially available conductive inks. These inks are typically capped with polymeric ligands that interfere with ink rheology and require high processing temperatures to achieve the desired electrical conductivity. For this reason, there is an impetus to develop conductive inks that can be processed at low temperatures in order to minimize processing costs and improve substrate compatibility. This work explores four methods of synthesizing silver nanoparticle based conductive inks, including polymeric ligand, ligand free, small molecule, and conductive ligand synthesis techniques.

Table of Contents

1. Introduction **1**

2. Synthesis of Thixotropic Inks for Direct Write Assembly **6**

2.1 Introduction 6

2.2 Experimental Techniques 8

2.2.1 Synthesis of Thixotropic Inks 8

2.2.2 Synthesis of Silver Nanoparticles Capped with 2,000 MW PAA 9

2.2.3 Synthesis of Silver Nanoparticles Capped with 100,000 MW PAA 9

2.2.4 Transmission Electron Microscopy 10

2.2.5 Scanning Electron Microscopy 10

2.2.6 Rheometry 10

2.3 Results and Discussion 11

2.4 Conclusion 15

3. Silver Nanoparticle Synthesis Techniques for the Decoupled Ink Synthesis Approach **16**

3.1 Introduction 16

3.2 Experimental Techniques 21

3.2.1 Synthesis of Ligand Free Nanoparticles 21

3.2.2 Synthesis of Nanoparticles Capped with Small Molecule Ligands 22

3.2.3 Synthesis of Nanoparticles Capped with Conductive Ligands 23

3.2.4 Transmission Electron Microscopy 24

3.2.5 Ultraviolet-Visible Optical Spectroscopy 25

3.2.6 Thermogravimetric Analysis 25

3.2.7 Stylus Profilometry 25

3.3 Results and Discussion 25

3.4 Conclusion 30

4. Conclusion and Future Work **31**

List of Figures

Figure 1.1: Direct write assembly of spanning, self-supporting electrodes, used to increase component packing density by routing wires over other wires. The extrusion nozzle is shown in green. 2

Figure 1.2: a.) Anode and cathode materials, shown in red and blue respectively, printed on planar gold electrodes via direct write assembly b.) Planar gold electrodes fabricated via traditional lithographic and electron beam deposition techniques 3

Figure 1.3: a.) Planar silver electrodes fabricated via inkjet printing of conductive silver inks b.) Anode and cathode materials, shown in red and blue respectively, with 3D silver electrodes printed in between to improve microbattery performance 4

Figure 1.4: The bulk conductivity of commercially available silver nanoparticle based inkjet printer inks, shown as a function of annealing/sintering temperature 5

Figure 2.3.1: a.) Transmission electron micrograph of a typical distribution of silver nanoparticles b.) Transmission electron micrograph of a typical distribution of silver nanoparticles, with bimodal particle size distribution evident 11

Figure 2.3.2: Transmission electron micrograph of a distribution of silver nanoparticles, representative of the lower mode of the bimodal particle size distribution, with average size of approximately 2 to 3 nm 11

Figure 2.3.3: a.) Scanning electron micrograph of a spanning planar sheet of sintered ink b.) Scanning electron micrograph of a spanning wire of sintered ink 12

Figure 2.3.4: Rheological properties of the various ink compositions 13

Figure 2.3.5: Viscosity profile of the undiluted (100 wt%) sample, with yield events shown 14

Figure 2.3.6: Synthesis of silver nanoparticles with 100K MW (left) and 2K MW (right) PAA 14

Figure 3.1.1: A schematic representation of a capped nanoparticle synthesis compared to a ligand free synthesis procedure, where the nanoparticles are shown as gray circles. 18

Figure 3.1.2: a.) trisodium citrate dihydrate b.) sodium benzoate c.) sodium dodecyl sulfate 18

Figure 3.3.1: a.) The reducing agent b.) The reaction vessel, immediately after the silver precursor is injected into the reducing agent c.) Aggregates of silver nanoparticles begin to form several minutes after the silver precursor is injected 26

Figure 3.3.2: An aggregate of ligand free silver nanoparticles (left). The inset view (right) shows unaggregated ligand free nanoparticles, with average particle size of 2 to 3 nm. 26

Figure 3.3.3: Ligand free silver nanoparticles aggregate into a macroscopic silver powder over the course of several days 27

Figure 3.3.4: Ultraviolet-visible optical spectroscopy data, with absorbance shown as a function of wavelength (left). The ink has a golden yellow appearance when diluted (right). 27

Figure 3.3.5: a.) Transmission electron micrographs, showing a.) a typical distribution of silver nanoparticles from ink 1 b.) two weakly aggregated particles c.) two spherical particles, with diameters of approximately 5 nm, which is representative of the average particle size 28

Figure 3.3.6: Thermogravimetric analysis data of the ink synthesized in Section 3.2.3 28

Figure 3.3.7: Thermogravimetric analysis data of the PEDOT:PSS gelled particles 29

Figure 3.3.7: Stylus profilometer depth map of a drop casted film, using a ink with minimal amounts of PEDOT:PSS 30

Figure 3.3.8: Stylus profilometer depth map of a drop casted film, using the ink synthesized in Section 3.2.3, with a significantly lower surface roughness 30

List of Tables

Table 2.2.1.1: Role of each reagent in the direct write assembly ink synthesis procedure 8

Table 2.2.6.1: Ink compositions for the dilution study 10

Table 3.2.1.1: Role of each reagent in the ligand free synthesis procedure 21

Table 3.2.2.1: Role of each reagent in the small molecule stabilized synthesis procedure 23

Table 3.2.3.1: Role of each reagent in the PEDOT:PSS stabilized synthesis procedure 24

1. Introduction

Advances in additive manufacturing technology over the past decade have allowed relatively inexpensive rapid prototyping systems to hit the commercial marketplace. Desktop three-dimensional (3D) printing technology, based on the fused filament fabrication process, is a prominent example that has significantly lowered the cost of rapid prototyping. 3D printers are capable of printing with millimeter accuracy and can produce shapes with complex geometries that could not otherwise be fabricated with conventional subtractive manufacturing or planar fabrication techniques. In most 3D printing processes, a 3D model is sliced into a series of lateral cross sections, which are then printed, layer by layer, to form the finished part. At present, additively-manufactured components are featured most prominently in structural applications, whereas its presence in printable electronics remains an emerging field with many novel application areas, including MEMS, microelectronics, sensors, and printed circuit boards, among others.[1–3]

Innovations in additively manufactured electronics have the potential to revolutionize integrated circuit and printed circuit board technology. In particular, current printed circuit board technology is constrained to planar, layered structures where component packing density is limited by in-plane wire routing. In small form factor portable electronics, miniaturization of printed circuit boards becomes increasingly important. To overcome the limits of existing printed circuit board technology and increase component packing density, there is a need to develop out-of-plane wire routing techniques. Direct write assembly, a 3D printing technology, is one such technique that can be used to print three-dimensional, spanning electrodes out of plane (**Figure 1.1**). More specifically, this technique utilizes a highly viscous, thixotropic and conductive ink to print three-dimensional, conductive structures to near net shape, with applications ranging from

printable spanning electrodes to antennas.[2,3] The main constituents of existing ink formulations are silver nanoparticles and polymeric additives, where the latter is used to tailor ink rheology.[2,3] When sintered, these inks maintain shape and form conductive silver structures.

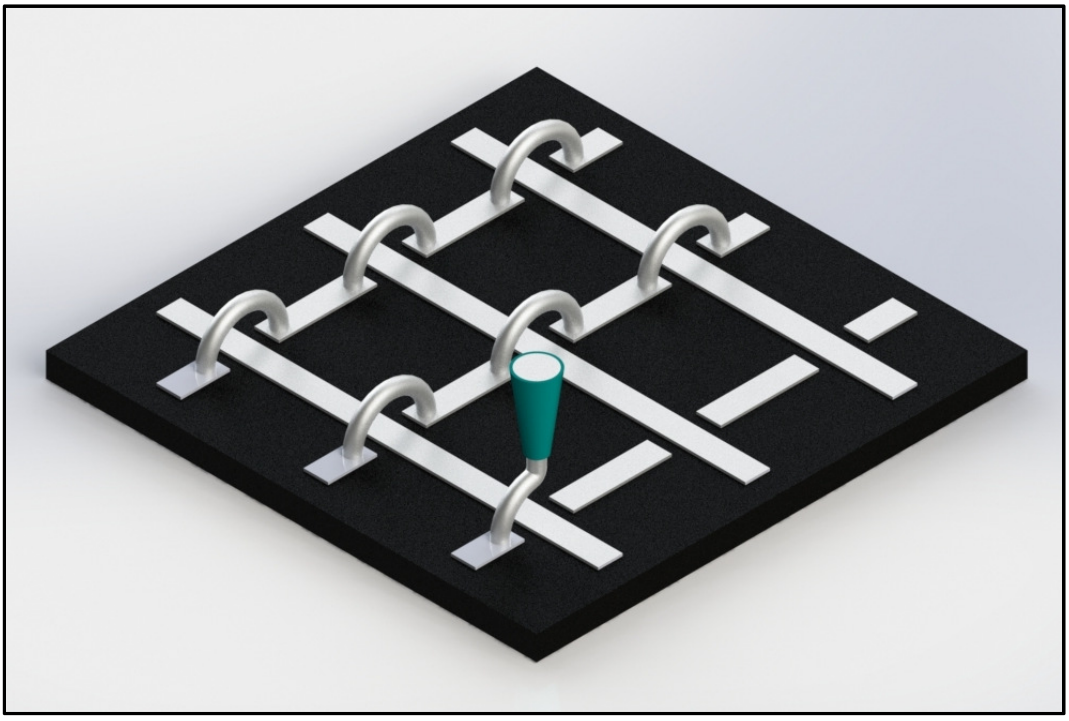

Figure 1.1: *Direct write assembly of spanning, self-supporting electrodes, used to increase component packing density by routing wires over other wires. The extrusion nozzle is shown in green.*

In addition to 3D printing of conductive silver structures, additive manufacturing of planar, conductive features can lower the cost of printed circuit board and integrated circuit development. By adjusting the composition and molecular weight (MW) of the polymeric additive, the ink rheology can be tailored towards a wide range of other printing technologies beyond direct write assembly, including doctor blading, drop casting and inkjet printing, among other applications. For example, inkjet printing of conductive silver traces can lower the upfront cost of developing prototype integrated circuits and printed circuit boards, where the cost of fabricating a lithographic mask set can be prohibitively expensive. More importantly, additively manufactured prototypes are functionally equivalent to their traditional counterparts, and can be

used to test performance and electromagnetic interference at a fraction of the cost prior to mass production. Printing conductive traces to net shape is also a more environmentally friendly process, as it eliminates the need for corrosive chemicals commonly found in etching, electroplating, and lithographic processes.

Beyond printing electrically conductive materials, it is also possible to print complete electronic devices. For example, Lewis and coworkers have successfully 3D printed a lithium ion microbattery with an interdigitated structure using direct write assembly, as shown in **Figure 1.2a**.[4] These microbatteries are produced by printing $Li_4Ti_5O_{12}$ and $LiFePO_4$ based inks on top of a planar, interdigitated electrode pattern (**Figure 1.2b**).[4] The 3D interdigitated structure of the battery, which cannot be produced with traditional manufacturing techniques, increases the effective anode/cathode interfacial area. As a result, 3D printed microbatteries can achieve significantly higher power densities compared to that produced by other manufacturing processes.[4]

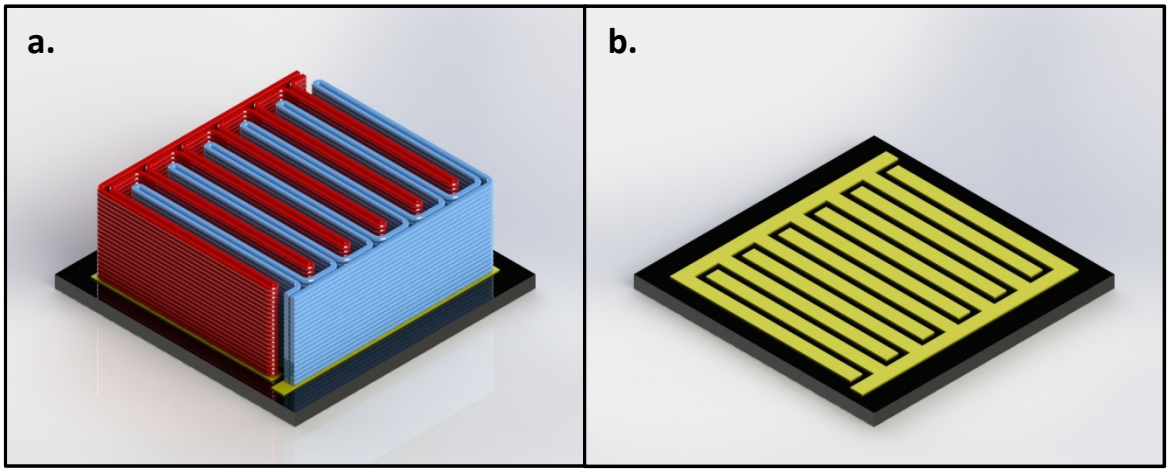

Figure 1.2: *a.) Anode and cathode materials, shown in red and blue respectively, printed on planar gold electrodes via direct write assembly b.) Planar gold electrodes fabricated via traditional lithographic and electron beam deposition techniques*

In addition, the capacity, current density, and power density can be optimized for specific applications by altering the battery's structure and dimensions; however, the maximum thickness

in the vertical dimension is limited by the parasitic resistance of the anode and cathode materials. Specifically, the current collection efficiency at the planar gold electrodes on the underside of the battery (**Figure 1.2b**), which were fabricated using traditional lithographic and electron beam deposition techniques, decreases with increasing vertical thickness.[4] As a result, the performance of existing 3D printed microbattery technology can be improved by additively manufacturing planar electrodes with 3D interconnects in conjunction with the anode and cathode materials, as shown in **Figure 1.3**.

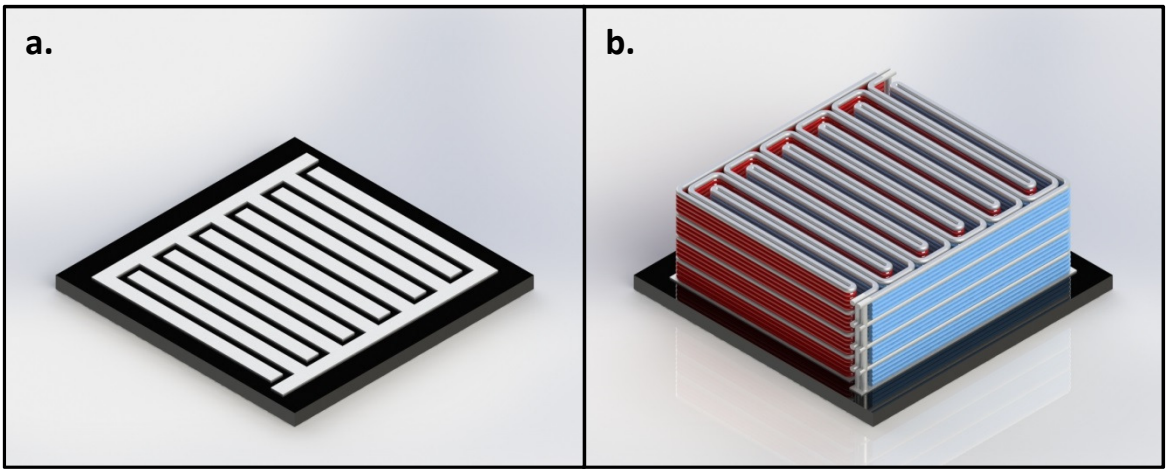

Figure 1.3: *a.) Planar silver electrodes fabricated via inkjet printing of conductive silver inks b.) Anode and cathode materials, shown in red and blue respectively, with 3D silver electrodes printed in between to improve microbattery performance*

In order to fully realize the benefits of additively manufactured electronics, high performance conductive inks must be developed to interface with the next generation of printed electronic devices. Existing conductive ink formulations require high annealing and sintering temperatures (**Figure 1.4**). To reduce ink production and development costs, these inks must be produced with high throughput synthesis techniques and tailorable rheological properties, so a single base ink can be used in a variety of printing applications. Likewise, the nanoparticle diameter must be minimized for a variety of reasons, most importantly, to mitigate nozzle clogging issues during printing and reduce the smallest printable feature size. In most ink

formulations, the nanoparticle diameter must be approximately two orders of magnitude smaller than that of the nozzle to avoid clogging issues.[1] Smaller nanoparticles have the added benefit of lower sintering temperatures, which decreases the energy required to post-process the ink after printing and improves compatibility with polymeric substrates that are susceptible to thermal degradation. The procedures outlined in Ahn *et al.* produced a nanoparticle size distribution of 5 to 50 nm, with a minimum printable feature size of ~2 µm.[2,3] While promising, the applications of this ink formulation are limited to the micrometer scale and thus incompatible with modern microfabrication technology. As a result, this work aims to provide an efficient means of printing the most fundamental building block of any electrical circuit, the wire, at the nanometer scale and at low temperatures to promote the development of printed electronic devices, which is hindered by the limitations of existing conductive ink technology at present.

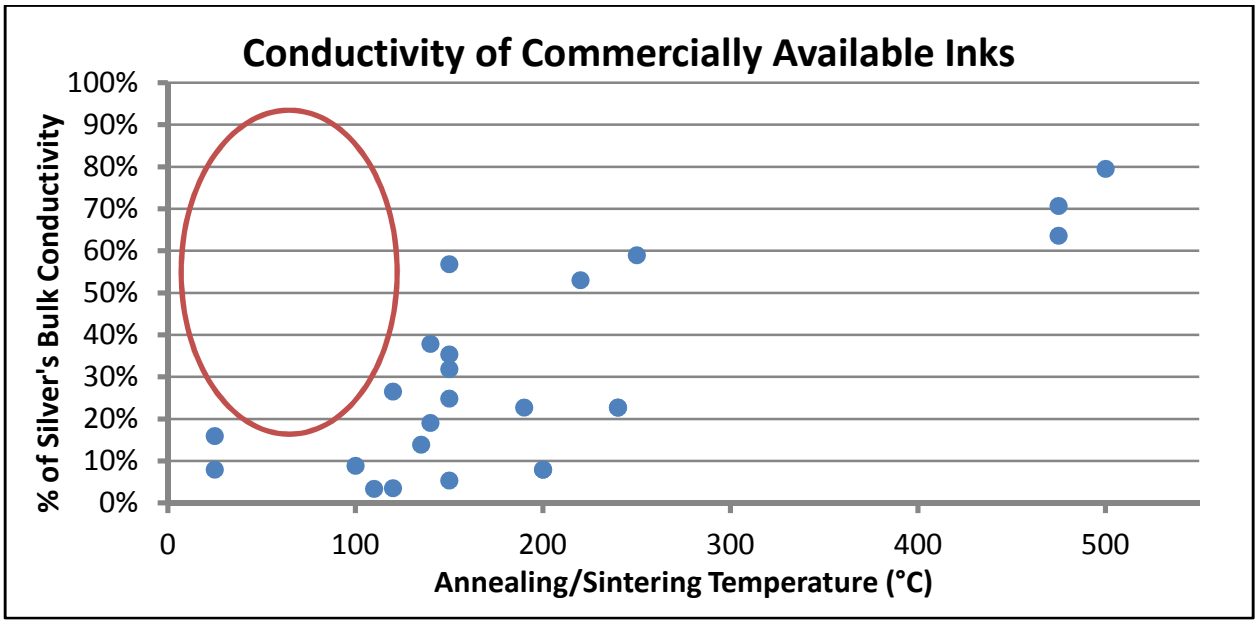

Figure 1.4: *The bulk conductivity of commercially available silver nanoparticle based inkjet printer inks, shown as a function of annealing/sintering temperature*

This work discusses the synthesis of silver nanoparticle based conductive inks, with applications ranging from direct write assembly to inkjet printing, and highlights a one-step synthesis procedure that produces an ink which exhibits conductivity when annealed at low

temperatures. Furthermore, this synthesis technique leverages a blend of conductive polymers and silver nanoparticles to tailor ink rheology for a range of potential applications, such as 3D printing with a high viscosity ink or printing transparent conducting electrodes with a low viscosity ink. We believe that this work will help establish a pathway towards printing of electrically conductive features at low temperatures and on the nanometer scale.

2. Synthesis of Thixotropic Inks for Direct Write Assembly

2.1 Introduction

Direct write assembly is a versatile 3D printing technology that uses colloidal inks to print a wide range of materials. For example, Kozin *et al.* used direct write assembly to print tympanic membrane grafts, with the eventual goal of replicating a human tympanic membrane and reversing hearing loss caused by damage to the tympanic membrane.[6] Direct write assembly has also been used to 3D print vascularized tissues, hydrogel scaffolds and hydroxyapatite scaffolds for biological applications.[7,8,9] As mentioned in **Section 1**, direct write assembly has been used to print electronic devices, including lithium ion microbatteries and electrically small antennas.[4,10,11] Recently, Skylar-Scott *et al.* has demonstrated a method of printing freestanding, conductive features with complex geometry.[12] In particular, a laser is used to sinter the silver nanoparticle based conductive ink as it exits the printer nozzle. Due to silver's high electrical and thermal conductivity, the underlying substrate material can be indirectly heated by the laser sintering process.[12] In some cases, the heat affected zone can be more than twice as wide as the conductive silver feature.[12] The authors tout this as favorable property, as it can be used to improve adhesion between the conductive silver feature and thermoplastic substrate.[12] However, it is important to note that this printing process cannot be used to print freestanding, conductive

features on thermally sensitive materials, such as those used in organic electronic devices, as doing so could degrade device performance.

Although the procedures developed by Ahn *et al.* have established a foundation for 3D printing conductive inks on the micron scale, the size of these printed features remains limited by the nanoparticle diameter, where printing smaller, nanometer-size features necessitates the synthesis of smaller nanoparticles in order to mitigate nozzle clogging issues.[2,3] The existing body of literature relating to silver nanoparticle synthesis focuses on producing high quality nanoparticles, at the expense of low throughput and yield, by mediating nanoparticle growth kinetics with polymeric ligands or low precursor concentrations.[3,5] In a typical aqueous nanoparticle synthesis procedure, a reducing agent is used to convert silver cations into metallic silver through the following reduction reaction: $Ag^+ + e^- \rightarrow Ag(s)$. Once silver seed crystallites have nucleated homogenously throughout the reaction mixture, further reduction occurs preferentially at the surface of the nanoparticle, causing it to grow. In order to control growth kinetics and achieve the desired nanoparticle size distribution, polymeric ligands are used to mediate the diffusion of Ag^+ cations to the surface of the nanoparticles. After the synthesis has reached completion, further nanoparticle growth must be quenched by removing unreacted silver precursor and reducing agent from the reaction vessel. Typically, this is achieved by diluting the nanoparticle solution with a solvent that the reducing agent and silver precursor are soluble in, but that the capping agent is not. In this way, the capped nanoparticles will rapidly precipitate out of solution. The resultant ink is then washed with various solvents via centrifugation and vacuum drying.

2.2 Experimental Techniques

2.2.1 Synthesis of Thixotropic Inks

In order to synthesize highly viscous and thixotropic conductive inks, a modified version of the method reported in Ahn *et al.*[2,3] was used. In particular, an aqueous solution of diethanolamine (DEA) and poly(acrylic acid) (PAA) was prepared in a round bottom flask using DEA (320 g, 3.04 mol), PAA (16 g, 5,000 MW, 50% aqueous solution), PAA (8 g, 50,000 MW, 25% aqueous solution) and deionized water (400 mL). The solution was then placed on a magnetic stir plate and stirred at 250 RPM. An aqueous silver nitrate ($AgNO_3$) solution was prepared in a separating funnel using $AgNO_3$ (160 g, 0.942 mol) and deionized water (160 mL). Following that, the aqueous $AgNO_3$ solution was dripped into the aqueous solution of DEA/PAA using the separating funnel. Once the addition was complete, the nucleation and growth of silver nanoparticles proceeded at room temperature for 24 h. The purpose of each reagent is described in **Table 2.2.1.1**. After 24 h elapsed, a 4 L beaker was filled with acetone (3 L), and the nanoparticle solution was subsequently poured into the beaker of acetone. After the nanoparticles precipitated from solution, the supernatant was decanted. The precipitate was collected and placed under vacuum to remove any remaining water and acetone from the paste.

Table 2.2.1.1: *Role of each reagent in the direct write assembly ink synthesis procedure*[2]

Reagent	**Role in Synthesis**
$AgNO_3$	Silver Precursor
poly(acrylic acid), 5,000 MW	Capping Agent
poly(acrylic acid), 50,000 MW	Capping Agent
DEA	Reducing Agent
deionized water	Solvent

2.2.2 Synthesis of Silver Nanoparticles Capped with 2,000 MW PAA

In order to synthesize silver nanoparticles capped with 2,000 MW PAA, an aqueous solution of DEA and 2,000 MW PAA was prepared in a 125 mL Erlenmeyer flask using DEA (10 g, 0.095 mol), PAA (2.5 g, 2,000 MW, 50% aqueous solution) and deionized water (11.25 mL). The solution was then placed on a magnetic stir plate and stirred at 250 RPM. An aqueous $AgNO_3$ solution was prepared in a separate beaker using $AgNO_3$ (5 g, 0.029 mol) and deionized water (5 mL). Following that, the aqueous $AgNO_3$ solution was poured into the aqueous solution of DEA/PAA, beginning nucleation and growth. After 24 h elapsed, ethanol (40 mL) was poured into the nanoparticle solution. After the nanoparticles precipitated from solution, the supernatant was decanted. The precipitate was collected and placed under vacuum to remove any remaining solvent from the paste.

2.2.3 Synthesis of Silver Nanoparticles Capped with 100,000 MW PAA

In order to synthesize silver nanoparticles capped with 100,000 MW PAA, an aqueous solution of DEA and 100,000 MW PAA was prepared in a 125 mL Erlenmeyer flask using DEA (10 g, 0.095 mol), PAA (3.57 g, 100,000 MW, 35% aqueous solution) and deionized (10.2 mL) water. The solution was then placed on a magnetic stir plate and stirred at 250 RPM. An aqueous $AgNO_3$ solution was prepared in a separate beaker using $AgNO_3$ (5 g, 0.029 mol) and deionized water (5 mL). Following that, the aqueous $AgNO_3$ solution was poured into the aqueous solution of DEA/PAA, beginning nucleation and growth. After 24 h elapsed, ethanol (40 mL) was poured into the nanoparticle solution. After the nanoparticles precipitated from solution, the supernatant was decanted. The precipitate was collected and placed under vacuum to remove any remaining solvent from the paste.

2.2.4 Transmission Electron Microscopy

The nanoparticles were imaged using a FEI Tecnai G2 F20 Supertwin transmission electron microscope. In particular, diluted nanoparticle solutions were drop casted on a copper grid, backed by a holey carbon support film, and vacuum dried in a glass scintillation vial overnight. In all experiments, the instrument was set to an acceleration voltage of 200 kV with a spot size of 3.

2.2.5 Scanning Electron Microscopy

Sintered films of silver nanoparticles were imaged using a JEOL 6010 scanning electron microscope. Samples were prepared by sintering the ink at 400 °C on a SiO_2-coated silicon substrate. The substrate was attached to the substrate holder using double sided carbon tape. The instrument was set to an acceleration voltage of 10 kV or 12 kV, with a spot size fixed at 30.

2.2.6 Rheometry

Ink rheology was characterized using an Anton Paar MCR 301 rheometer, operated in stress controlled mode, to measure ink viscosity as a function of shear rate. Five samples of varying concentrations were prepared following the ink compositions shown in **Table 2.2.6.1**. All experiments used the PP25 parallel-plate measuring system, with a 1 mm inter-plate spacing. The temperature of the dilution study was maintained at 25 °C with a thermoelectric heat pump.

Table 2.2.6.1: *Ink compositions for the dilution study*

Ink Concentration (weight percent)	Ink Concentration (g ink / mL water)
100 wt%	infinity
80 wt%	4.00 g/mL
60 wt%	1.50 g/mL
40 wt%	0.67 g/mL
20 wt%	0.25 g/mL

2.3 Results and Discussion

The optimized synthesis method, described in **Section 2.2.1**, produces a bimodal particle size distribution, with particle sizes ranging from 2 to 50 nm (**Figures 2.3.1 and 2.3.2**). The lower and higher modes appear at approximately 2.5 nm and 15 nm, respectively. Even though both synthesis procedures result in a similar range of particle sizes, it is important to note that this optimized method produces a significantly higher number density of smaller nanoparticles than that reported in Ahn *et al.* (**Figure 2.3.2**).[2,3]

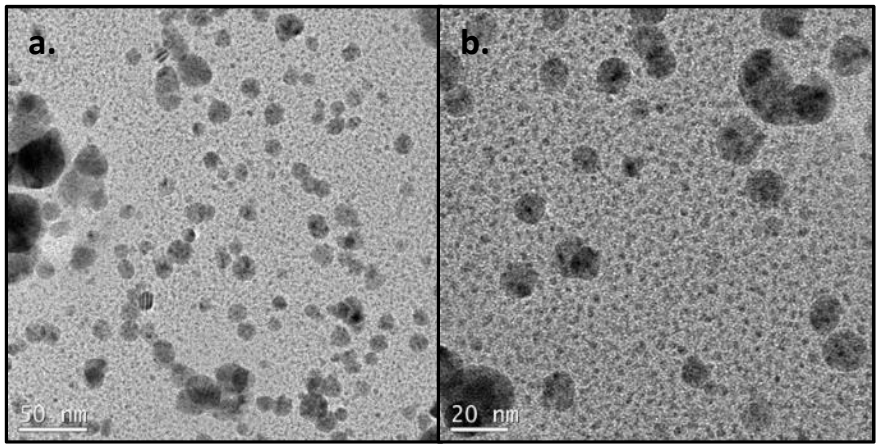

Figure 2.3.1: *a.) Transmission electron micrograph of a typical distribution of silver nanoparticles b.) Transmission electron micrograph of a typical distribution of silver nanoparticles, with bimodal particle size distribution evident*

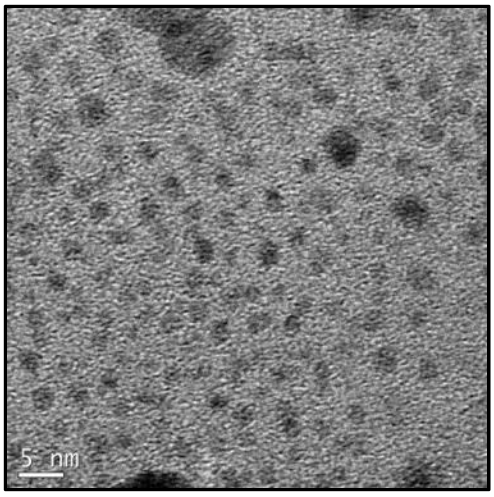

Figure 2.3.2*: Transmission electron micrograph of a distribution of silver nanoparticles, representative of the lower mode of the bimodal particle size distribution, with average size of approximately 2 to 3 nm*

When sintered, the ink has a porous structure that is typical of most sintered powders (**Figure 2.3.3**). The highly porous nature of the sintered ink can be attributed to outgassing of residual solvent and byproducts of the thermal decomposition reaction of PAA. These pores adversely affect the conductivity of the sintered silver nanoparticle paste by increasing grain boundary scattering and reducing the effective cross-sectional area of the silver electrode. Even so, the sintered ink shows conductance typical of printed circuit boards, as verified by a digital multimeter in continuity test mode.

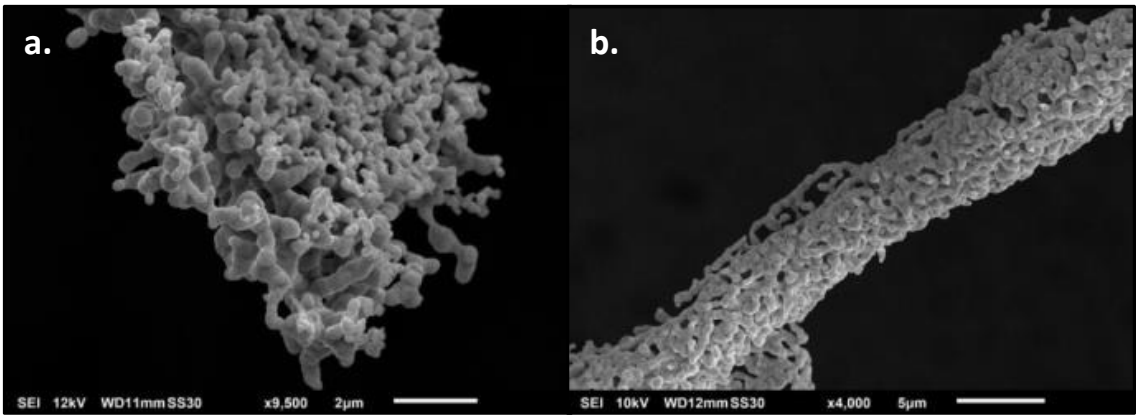

Figure 2.3.3: *a.) Scanning electron micrograph of a spanning planar sheet of sintered ink b.) Scanning electron micrograph of a spanning wire of sintered ink*

In order to characterize the ink rheology, a rheometer was used to measure the ink's viscosity as a function of shear rate, as discussed in **Section 2.2.6**. The results of the dilution study are shown in **Figure 2.3.4**. Of the five samples, only the undiluted ink sample shows thixotropic behavior (**Figures 2.3.4 and 2.3.5**). The zero shear viscosity of the undiluted ink is extremely high, which enhances the ink's self-supporting ability. In particular, longer spanning and unsupported electrodes can be printed with increasing zero shear viscosity. At ink concentrations of 80 wt% or below, the ink appears to behave like a Newtonian fluid and can be used in other printing applications beyond direct write assembly, such as inkjet printing. As a

result, the rheological properties of this ink can be tailored towards a wide range of printing technologies, by simply diluting the concentrated ink with water.

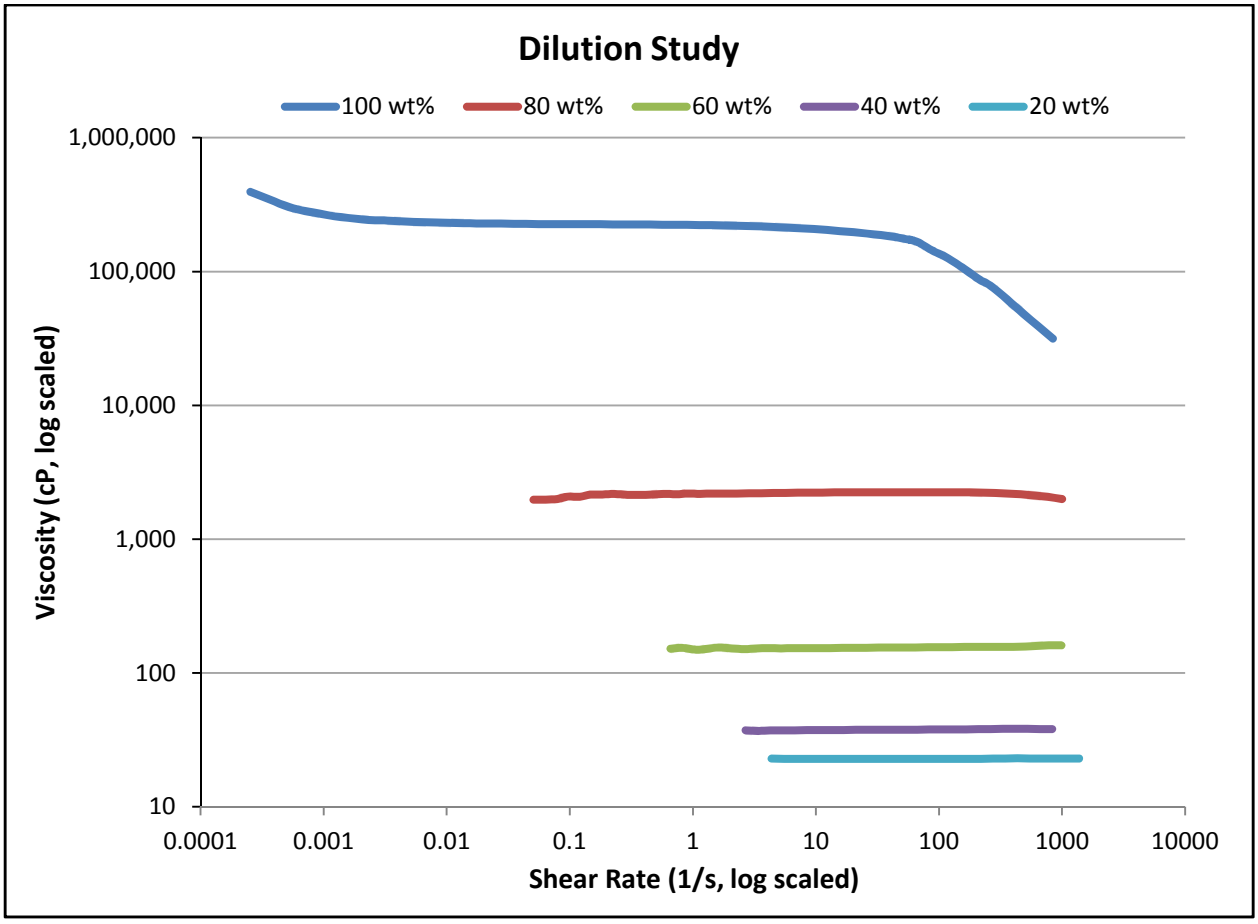

Figure 2.3.4: *Rheological properties of the various ink compositions*

It is important to note that the viscosity profile of the undiluted ink shows that the ink yields at two locations, one at low shear rates and the other at a shear rate of approximately 50 1/s (**Figure 2.3.5**). This rheological behavior is consistent with the bimodal molecular weight distribution of PAA. Specifically, the first yield event corresponds to the yielding of the higher molecular weight PAA (50,000 MW), as it takes less shear stress to align longer polymer chains. Similarly, the second yield event corresponds to the yielding of the lower molecular weight PAA (5,000 MW), as it takes more shear stress to align shorter polymer chains. In order to maximize the thixotropic behavior of the ink, the amount of 5,000 MW PAA must be minimized.

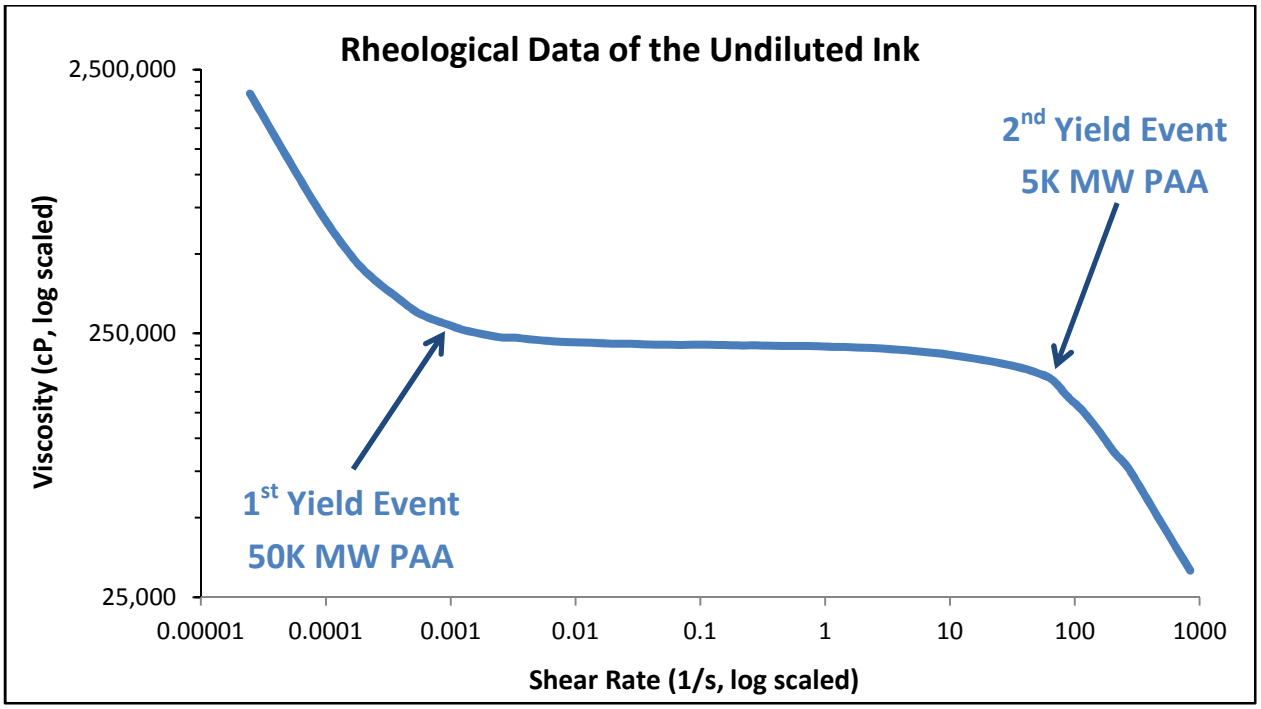

Figure 2.3.5: *Viscosity profile of the undiluted (100 wt%) sample, with yield events shown*

Reducing the molecular weight of the 5,000 MW PAA is a non-trivial task. Namely, the molecular weight of the capping agent is tied to the growth kinetics of the nanoparticles during synthesis as discussed in **Section 2.1**. The nanoparticle solutions, synthesized in **Sections 2.2.2 and 2.2.3**, demonstrate the effect of molecular weight on the growth kinetics of the silver nanoparticles (**Figure 2.3.6**).

Figure 2.3.6: *Synthesis of silver nanoparticles with 100K MW (left) and 2K MW (right) PAA*

The absorption intensity in the 100,000 MW PAA synthesis is significantly stronger, which can be attributed to an increased number of nanoparticles in the 100,000 MW synthesis relative to the 2,000 MW synthesis. With approximately fifty times less stabilizing ligands than the 2,000 MW synthesis, the nucleation and growth of the silver nanoparticles proceeded at a faster rate in the 100,000 MW synthesis. Thus, it is clear that the 5,000 MW PAA is the rate controlling capping agent of the synthesis procedure outlined in **Section 2.2.1**. More importantly, reducing or removing the 5,000 MW PAA from the synthesis procedure would lead to larger and more undesirable nanoparticles.

2.4 Conclusion

The synthesis technique outlined in **Section 2.2.1** produces a bimodal distribution of silver nanoparticles and yields a considerably higher number density of small nanoparticles, with a diameter of 2 - 3 nm, than previously reported synthesis techniques.[2,3] This method offers a promising route towards 3D printing electronic devices on the nanometer scale, where small particles are needed to avoid nozzle clogging issues during printing. Data from the rheometry experiments performed in **Section 2.2.6** shows thixotropic behavior and an extremely high zero shear viscosity in the undiluted sample, which indicates that this ink can potentially be used to produce self-supported, 3D printed structures. The ink also exhibits tailorable rheological properties when diluted with water and is thus compatible with other printing applications, such as inkjet printing, when diluted to the appropriate viscosity.

It is important to note that the viscosity profile shows two yield events, which corresponds to the bimodal molecular weight distribution of PAA. Though the 5,000 MW PAA inhibits growth kinetics of the nanoparticles and reduces particle size, it simultaneously increases the shear rate necessary to extrude the ink through a nozzle (**Figure 2.3.5**). Results from **Figure**

2.3.6 show that adjusting the composition of the PAA capping agent can adversely affect the growth kinetics of the silver nanoparticles; thus, there is motivation to develop other synthesis approaches that would allow precise control of the ink's rheological properties and nanoparticle size distribution. In **Section 3** below, we investigate three alternative nanoparticle synthesis approaches, the ligand-free, small molecule, and conductive ligand synthesis techniques. More specifically, silver nanoparticles with controlled size and distribution would first be synthesized using one of the aforementioned synthesis approaches. Once the silver nanoparticle synthesis procedure is optimized, polymer additives will be introduced to the system to tailor ink rheology to the desired application, allowing one base ink that is produced in bulk to be implemented across a range of technical applications. For example, low-cost transparent conducting electrodes could be manufactured by printing a lower viscosity ink in a nanometer scale grid pattern on top of a transparent substrate. This conductive ink design strategy can be implemented across a wide range of applications, whether for highly viscous inks used to manufacture self-supporting, conductive 3D structures, or low viscosity inks used in inkjet printing of additively manufactured electrodes.

3. Silver Nanoparticle Synthesis Techniques for the Decoupled Ink Synthesis Approach

3.1 Introduction

The decoupled ink synthesis approach addresses the need to isolate the rheological properties from ink synthesis. By synthesizing silver nanoparticles with a minimal amount of capping agents, the ink rheology can be tailored towards the desired application post-synthesis without adversely affecting the nanoparticle synthesis. Silver nanoparticles can be synthesized through a variety of methods. In Naidu *et al.*, silver nanoparticles were synthesized *in situ* in the active layer of a bulk heterojunction solar cell.[13] In particular, $AgNO_3$ and poly(ethylene glycol),

the silver precursor and reducing agent respectively, were dissolved into the active layer of the solar cell.[13] When annealed at elevated temperatures, the hot plate provides the thermal energy necessary to nucleate and grow silver nanoparticles *in situ* in the active layer. Other techniques leverage reactive silver inks, where nanoparticles are synthesized on-the-fly as the ink dries.[14,15] Reactive silver inks contain dissolved silver complexes and reducing agents. The reducing agent becomes active when the ink dries, and subsequently reduces the silver complexes into silver nanoparticles.[15] For this reason, reactive silver inks can be printed as a liquid, where nanoparticle synthesis occurs as the ink is drying on the substrate. The most common silver nanoparticle synthesis method produces silver nanoparticles in solution by chemically reducing aqueous silver cations into nanoparticles, as described in the paragraphs below. In this section, three different solution-based nanoparticle synthesis techniques are explored, the ligand free, small molecule, and conductive ligand approaches. All of these synthesis techniques are compatible with the decoupled ink production methodology described previously.

In a typical ligand free synthesis, silver nanoparticles are synthesized by injecting the silver precursor, an aqueous solution of $AgNO_3$, into a flask filled with the reducing agent, an aqueous solution of sodium borohydride ($NaBH_4$). The silver nanoparticles are synthesized through the following reduction reaction in a controlled nitrogen atmosphere: $AgNO_3 + NaBH_4 + 3H_2O \rightarrow Ag(s) + H_3BO_3 + NaNO_3 + \frac{7}{2}H_2$.[16] Ligand free synthesis techniques afford numerous benefits compared to traditional nanoparticle synthesis procedures, as shown in **Figure 3.1.1**. In absence of organic ligands, the silver precursor is rapidly consumed during the nucleation processed followed by little to no growth. As a result, small nanoparticles can be synthesized at a high throughput and concentration using this method.

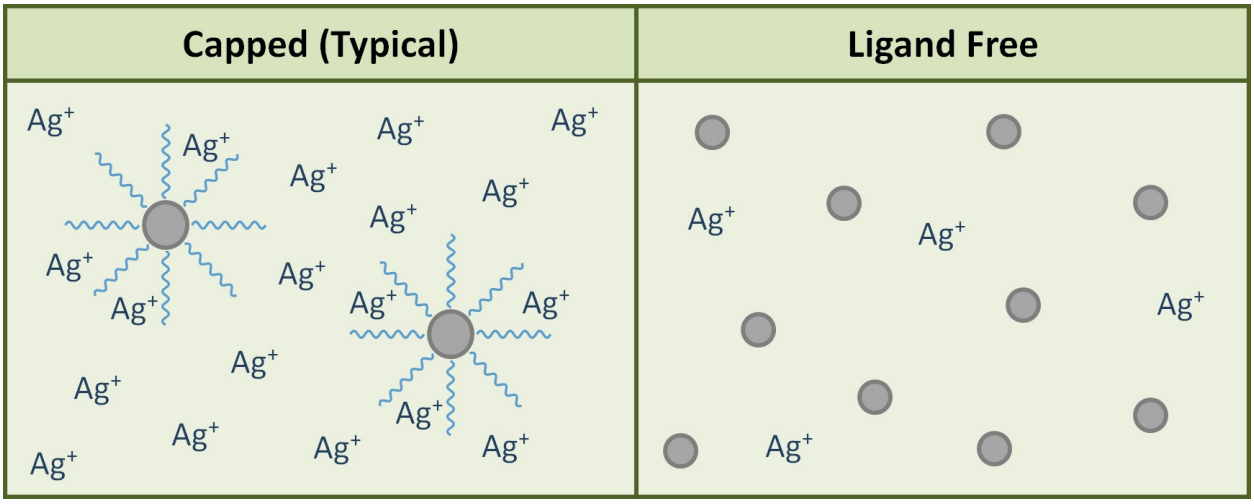

Figure 3.1.1: *A schematic representation of a capped nanoparticle synthesis compared to a ligand free synthesis procedure, where the nanoparticles are shown as gray circles.*

The small molecule synthesis approach extends the ligand free synthesis technique by introducing small molecule capping agents into the reaction vessel. Examples include trisodium citrate dihydrate, sodium benzoate, and sodium dodecyl sulfate (**Figure 3.1.2**). These molecules contain anionic functional groups, such as carboxylates and sulfates, which ligate the surface of the nanoparticle via coulombic attraction. Due to their short effective lengths, small molecule ligands have a minimal effect on ink rheology.

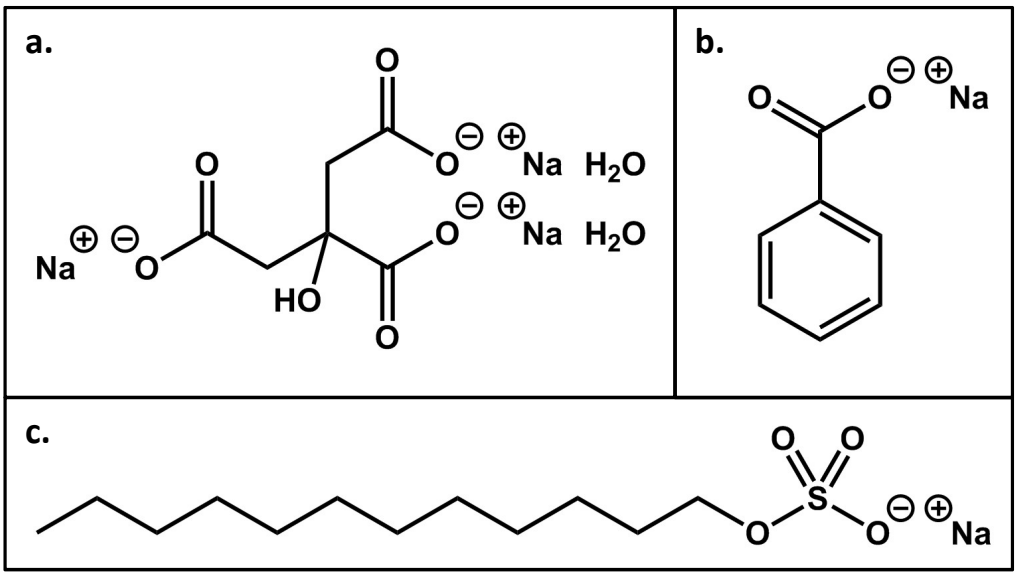

Figure 3.1.2: *a.) trisodium citrate dihydrate b.) sodium benzoate c.) sodium dodecyl sulfate*

The ligands shown in **Figure 3.1.2** have many favorable properties. In particular, they are inexpensive, environmentally benign, and contain anionic functional groups. Sodium benzoate and trisodium citrate dihyrdate are common food additives, and sodium dodecyl sulfate is a household surfactant that is commonly found in shampoos and other commercially available cleaning agents. Compared to ligand free nanoparticles, nanoparticles capped with small molecule ligands are less susceptible to agglomeration and tend to exhibit longer shelf lives. In addition, these ligands have been used extensively throughout the nanoparticle synthesis literature. For example, trisodium citrate has been used both as a capping and reducing agent.[17] Nanoparticles as small as 20 nm have been synthesized using trisodium citrate and $NaBH_4$ as the capping and reducing agent, respectively.[18,19] Tang *et al.* synthesized sodium dodecyl sulfate capped nanoparticles using a $NaBH_4$ reduction strategy.[20] This synthesis procedure is capable of producing nanoparticles with average sizes ranging from 2 nm to 34 nm, where the particle size distribution can be tuned by adjusting the duration of the synthesis procedure.[20] It is important to note that the aforementioned synthesis procedures tend to produce nanoparticle solutions at concentrations much lower than practical printing concentrations. In order to synthesize a high concentration of small molecule stabilized nanoparticles, an approach that leverages a combination of ligands must be used.

In the final synthesis approach, conductive polymers are used to ligate the nanoparticles during synthesis. In particular, the conductive ligand synthesis approach leverages poly(3,4-ethylenedioxythiophene):poly(styrenesulfonate) (PEDOT:PSS), a well-studied conductive polymer that is widely used throughout the research community. PEDOT:PSS is a water soluble blend of PEDOT and PSS, which contains anionic sulfonate functional groups that can coordinate with the surface of the silver nanoparticles. Nanoparticles that are ligated with

PEDOT:PSS have a significantly higher solubility in water. Compared to the ligand free and small molecule synthesis approaches, the resultant ink has a longer shelf life and is compatible with low temperature processes, as thermal decomposition is not required to achieve conductivity. Adding to that, gelled PEDOT:PSS particles serve as a polymeric binder, thus improving film conformity and reducing thermal cracking.

To date, many research groups have leveraged a layered structure of PEDOT:PSS and silver to print transparent conducting electrodes for organic photovoltaic applications. In particular, these transparent conducting electrodes are created by printing silver finger electrodes or grids on films of PEDOT:PSS with a variety of printing technologies, including flexographic, inkjet and roll-to-roll printers.[21,22,23,24,25,26,27] Commercially available inks can be used to print the silver and PEDOT:PSS layers, reducing the cost of ink development; however, device performance is often limited by the capabilities of existing ink formulations. For example, cracking in printed silver films limited the performance of the organic photovoltaic devices produced in Franeker *et al*.[25] In addition, Georgiou *et al.* noted that their silver nanoparticle inks had a tendency to diffuse into films of PEDOT:PSS during printing, degrading the overall performance of their organic photovoltaic devices.[23] Other research has focused on using silver nanoparticles to improve the conductivity of PEDOT:PSS, but not vice versa. For example, some authors have improved the conductivity of PEDOT:PSS by mixing solutions of PEDOT:PSS and silver nanoparticles together.[28,29] Park *et al.* employed a similar strategy to improve the performance of organic light emitting diodes.[30] It has also been shown that PEDOT is capable of reducing Ag^{+} cations into silver nanoparticles.[31,32,33,34] Moreno *et al.* reported an increase in conductivity of three orders magnitude by synthesizing silver nanoparticles in the presence of PEDOT:PSS and $NaBH_4$.[35] It is important to note that a mass ratio of 100:1 (PEDOT:PSS to

$AgNO_3$) was used in this study.[35] In contrast, we seek to develop a hybrid ink that has comparable conductivity to bulk silver by leveraging high concentrations of silver nanoparticles and minimal amounts of PEDOT:PSS.

3.2 Experimental Techniques

3.2.1 Synthesis of Ligand Free Nanoparticles

Ligand free silver nanoparticles were synthesized following a modified version of the synthesis procedure found in Wani *et al*.[16] An aqueous solution of the reducing agent was prepared in a 1000 mL 3-neck round-bottom flask using $NaBH_4$ (0.378 g, 0.01 mol) and deionized water (245 mL). The 3-neck round-bottom flask was placed on a magnetic stir plate and stirred at 1000 RPM. In addition, the flask was connected to a Schlenk line and the ambient atmosphere in the flask was displaced with nitrogen. The remaining necks were then closed off with rubber septa. An aqueous $AgNO_3$ solution was prepared in a separate beaker using $AgNO_3$ (3.4 g, 0.02 mol) and deionized water (5 mL). The $AgNO_3$ solution was briefly placed in an ultrasonic bath to accelerate the dissolution process. A 10 mL syringe, tipped with a 16 gauge needle, was used to inject the $AgNO_3$ solution into the reducing agent solution, initiating the ligand free synthesis. The nanoparticle nucleation and growth process occurred over the course of several seconds. The nanoparticles aggregated into clusters that precipitated from solution after several minutes. The supernatant was decanted and the nanoparticles were collected. The role of each reagent in this synthesis procedure is summarized in **Table 3.2.1.1**.

Table 3.2.1.1: *Role of each reagent in the ligand free synthesis procedure*

Reagent	**Role in Synthesis**
$AgNO_3$	Silver Precursor
$NaBH_4$	Reducing Agent
deionized water	Solvent

3.2.2 Synthesis of Nanoparticles Capped with Small Molecule Ligands

Silver nanoparticles, capped with small molecule ligands, were synthesized based on the procedure found in **Section 3.2.1**. An aqueous solution of the reducing agent was prepared in a 1000 mL 3-neck round-bottom flask using $NaBH_4$ (0.378 g, 0.01 mol), trisodium citrate dihydrate (5.882 g, 0.02 mol), sodium benzoate (2.882 g, 0.02 mol), sodium dodecyl sulfate (0.288 g, 0.001 mol), n-butanol (25 mL), ethanol (25 mL) and deionized water (245 mL). The 3-neck round-bottom flask was placed on a magnetic stir plate and stirred at 1000 RPM. In addition, the flask was connected to a Schlenk line and the ambient atmosphere in the flask was displaced with nitrogen. The remaining necks were then closed off with rubber septa. An aqueous $AgNO_3$ solution was prepared in a separate beaker using $AgNO_3$ (3.4 g, 0.02 mol) and deionized water (5 mL). The $AgNO_3$ solution was briefly placed in an ultrasonic bath to accelerate the dissolution process. A 10 mL syringe, tipped with a 16 gauge needle, was used to inject the $AgNO_3$ solution into the reducing agent solution, initiating nanoparticle synthesis. After 1 h elapsed, acetone (700 mL) was added to the reaction vessel. The nanoparticles, capped with citrate, benzoate, and dodecyl sulfate ligands, are weakly soluble in acetone and readily precipitate from solution. Once the nanoparticles precipitated from solution, the supernatant was decanted. The precipitate was collected in a centrifuge tube and centrifuged three times at 8000 RPM to separate the larger nanoparticles from the smaller nanoparticles. In each successive centrifugation step, the supernatant was collected and the pellet was redispersed in deionized water. The supernatant, referred to as ink 1 henceforth, contains a lower concentration of the smallest nanoparticles. The pellet from the final centrifugation step was dispersed in deionized water, forming ink 2, which is more concentrated and contains larger nanoparticles. The role of each reagent in this synthesis procedure is summarized in **Table 3.2.2.1**.

***Table 3.2.2.1**: Role of each reagent in the small molecule stabilized synthesis procedure*

Reagent	Role in Synthesis
$AgNO_3$	Silver Precursor
trisodium citrate dihydrate	Capping Agent
sodium benzoate	Capping Agent
sodium dodecyl sulfate	Capping Agent
ethanol	Defoamer
n-butanol	Defoamer
$NaBH_4$	Reducing Agent
deionized water	Solvent

It is important to note that sodium dodecyl sulfate, being a surfactant, has the propensity to bubble and foam. This silver nanoparticle synthesis procedure evolves hydrogen gas, as discussed in **Section 3.1**. If left unchecked, the reaction mixture will violently foam and force the nanoparticle solution out of the flask through any pressure relief mechanism, such as a rubber septum or Schlenk line. For this reason, alcohols were added to the reaction mixture as a defoaming agent, to prevent the reaction mixture from bubbling out of the flask. A defoamer is any solvent that can reduce the surface tension of the reaction mixture, causing bubbles to pop faster. Ethanol and n-butanol were selected based upon qualitative comparison of many solvents, including ethanol, n-butanol, isopropanol, octanol, methyl ethyl ketone, ethylene glycol, diethylene glycol, triethylene glycol monomethyl ether, and polyethylene glycol.

3.2.3 Synthesis of Nanoparticles Capped with Conductive Ligands

Silver nanoparticles, capped with PEDOT:PSS gelled particles, were synthesized based on the procedures found in **Sections 3.2.1 and 3.2.2**. An aqueous solution of the reducing agent was prepared in a 1000 mL 3-neck round-bottom flask using $NaBH_4$ (0.378 g, 0.01 mol), PEDOT:PSS gelled particles (10.74 g) and deionized water (112 mL). The 3-neck round-bottom flask was placed on a magnetic stir plate and stirred at 400 RPM. In addition, the flask was connected to a Schlenk line and the ambient atmosphere in the flask was displaced with nitrogen.

The remaining necks were then closed off with rubber septa. An aqueous $AgNO_3$ solution was prepared in a separate beaker using $AgNO_3$ (1.7 g, 0.01 mol) and deionized water (2 mL). The $AgNO_3$ solution was briefly placed in an ultrasonic bath to accelerate the dissolution process. A 10 mL syringe, tipped with a 16 gauge needle, was used to inject the $AgNO_3$ solution into the reducing agent solution, initiating nanoparticle synthesis. After 30 min elapsed, acetone (800 mL) was added to the reaction vessel. The nanoparticles, capped with PEDOT:PSS ligands, are weakly soluble in acetone and readily precipitate from solution. Once the nanoparticles precipitated from solution, the supernatant was decanted. The precipitate was collected in a centrifuge tube, dispersed in acetone and deionized water, and centrifuged at 12,000 RPM to separate the nanoparticles and PEDOT:PSS from the solvent. The pellet was collected from the centrifuge tube and redispersed in 10 mL of deionized water. The silver nanoparticle and PEDOT:PSS solution was then placed under vacuum briefly to remove any residual acetone. The role of each reagent in this synthesis procedure is summarized in **Table 3.2.3.1**.

Table 3.2.3.1: *Role of each reagent in the PEDOT:PSS stabilized synthesis procedure*

Reagent	**Role in Synthesis**
$AgNO_3$	Silver Precursor
PEDOT:PSS gelled particles	Capping Agent
$NaBH_4$	Reducing Agent
deionized water	Solvent

3.2.4 Transmission Electron Microscopy

The nanoparticles were imaged using a FEI Tecnai G2 F20 Supertwin transmission electron microscope. In particular, diluted nanoparticle solutions were drop casted on a copper grid, backed by a holey carbon support film, and vacuum dried in a glass scintillation vial overnight. In all experiments, the instrument was set to an acceleration voltage of 200 kV with a spot size of 3.

3.2.5 Ultraviolet-Visible Optical Spectroscopy

The optical absorbance spectrum of diluted nanoparticle solutions was measured using a ThermoFisher EVO350 spectrometer. Each sample was placed in a polystyrene cuvette and the optical absorbance spectrum was measured using a reference of deionized water.

3.2.6 Thermogravimetric Analysis

Thermogravimetric weight loss data was measured using a TA Instruments thermogravimetric analyzer. In all experiments, the following temperature ramp profile was used: ramp to 80 °C at 10 °C/min, hold at 80 °C for 30 min and ramp to 500 °C at 5 °C/min. All experiments were carried out in medical grade air.

3.2.7 Stylus Profilometry

Topographical maps of dried films were measured using a Bruker OM-DektakXT stylus profilometer. Inks were drop casted onto a SiO_2-coated silicon substrate and measured using a 2 μm diameter diamond stylus. The instrument was operated in constant force mode.

3.3 Results and Discussion

The ligand free synthesis method, outlined in **Section 3.2.1**, produces a significantly higher concentration of smaller nanoparticles over the span of several seconds compared to the procedure discussed in **Section 2.2.1**. In addition to high throughput and yield, this synthesis technique produces nanoparticles with a ligand free surface, a favorable ink property. In particular, nanoparticles with ligand free surfaces can be annealed at low temperatures, unlike conventional nanoparticles capped with polymeric ligands, where high temperature processing is required to thermally decompose ligands. When dried, ligand free nanoparticles tend to produce films with higher conductivities, as these films do not have any residual carbon in between nanoparticles.

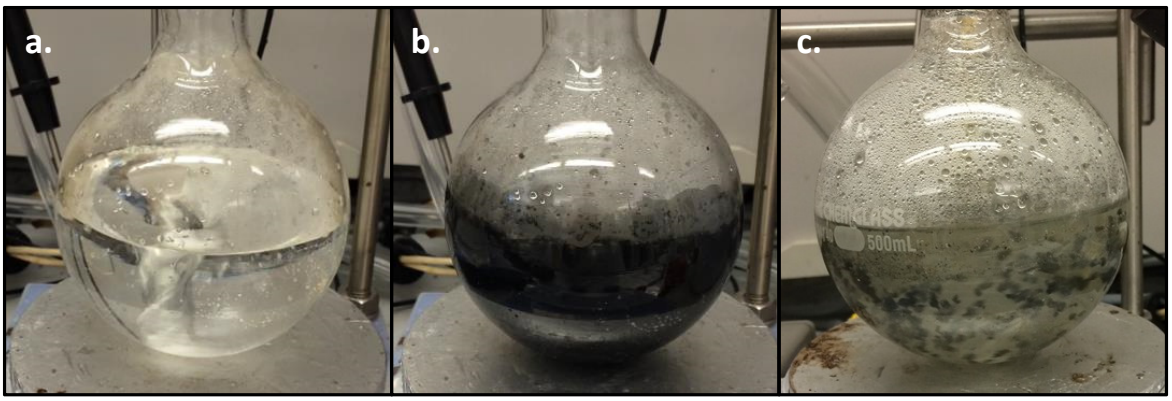

Figure 3.3.1: *a.) The reducing agent b.) The reaction vessel, immediately after the silver precursor is injected into the reducing agent c.) Aggregates of silver nanoparticles begin to form several minutes after the silver precursor is injected*

When the silver precursor is injected into the reducing agent (**Figure 3.3.1a**), the reaction mixture turns black immediately as shown in **Figure 3.3.1b**, which indicates the formation of a high concentration of silver seed crystallites. Several minutes after injection, the silver nanoparticles begin to aggregate into clusters as shown in **Figure 3.3.1c**. Without organic ligands to prevent surface interactions between nanoparticles, the nanoparticles tend to aggregate to reduce surface energy. **Figure 3.3.2** shows a large aggregate, with small nanoparticles clustered around the main aggregate. The unaggregated nanoparticles are approximately 2 to 3 nm, which is an extremely favorable particle size for nanoscale printing applications.

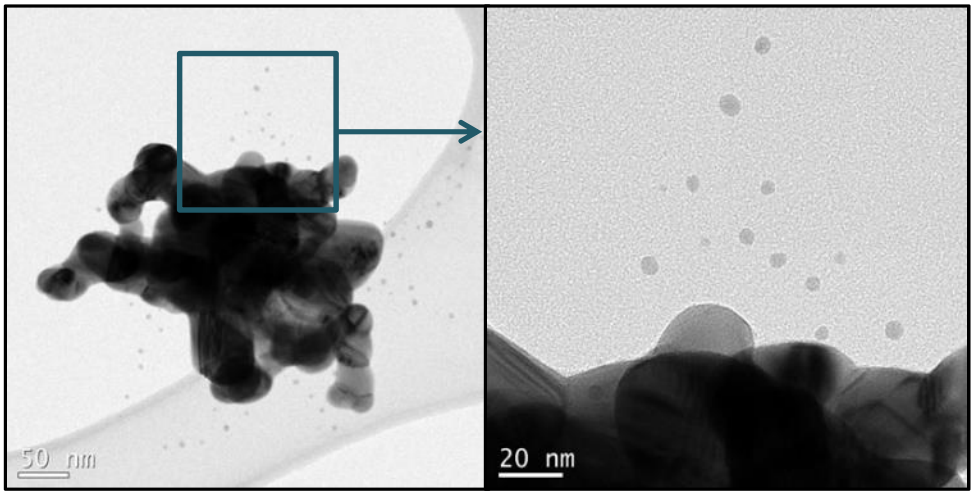

Figure 3.3.2: *An aggregate of ligand free silver nanoparticles (left). The inset view (right) shows unaggregated ligand free nanoparticles, with average particle size of 2 to 3 nm.*

However, agglomeration is an ongoing issue, where the nanoparticles tend to aggregate into a macroscopic silver powder over the course of several days (**Figure 3.3.3**). As a result, organic ligands are necessary in order to reduce nanoparticle agglomeration and improve ink shelf life.

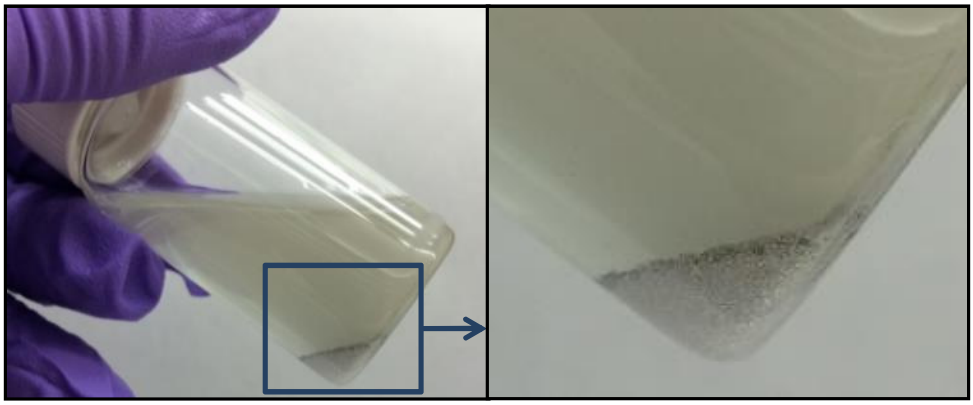

Figure 3.3.3: *Ligand free silver nanoparticles aggregate into a macroscopic silver powder over the course of several days*

The small molecule stabilized nanoparticles produced in **Section 3.2.2** exhibit a higher colloidal stability and improved shelf life. The ultraviolet-visible optical spectroscopy data (**Figure 3.3.4**) shows a narrow absorbance peak centered at 395 nm, which is indicative of a narrow particle size distribution and an average particle size that is below 10 nm.[36]

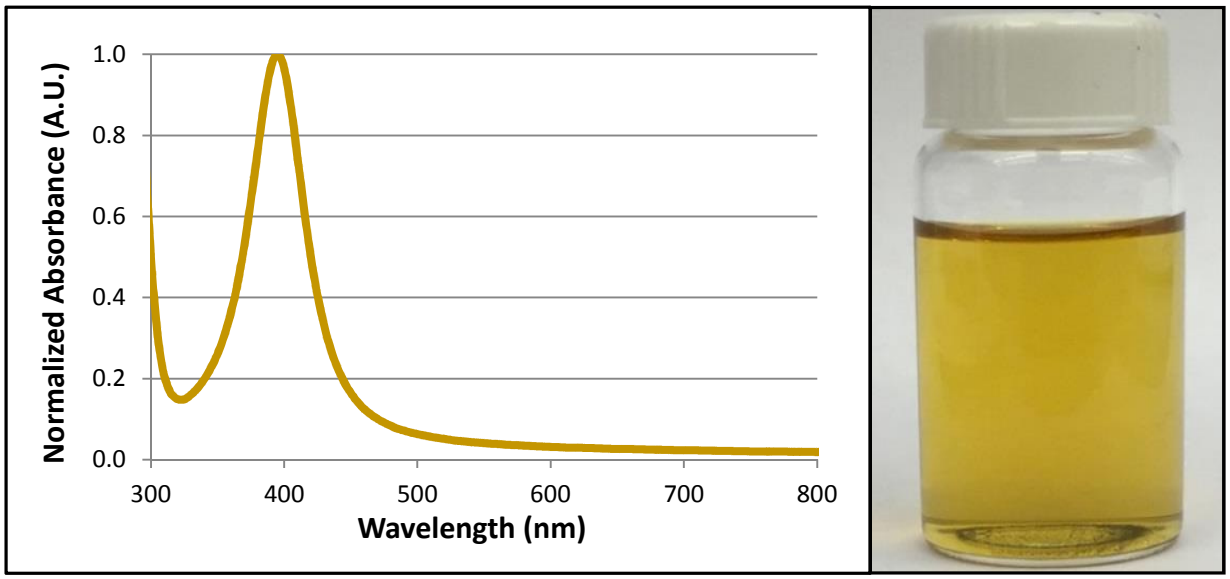

Figure 3.3.4: *Ultraviolet-visible optical spectroscopy data, with absorbance shown as a function of wavelength (left). The ink has a golden yellow appearance when diluted (right).*

These findings were confirmed with the transmission electron micrographs shown in **Figure 3.3.5** below. **Figures 3.3.5a and 3.3.5b** both show weakly aggregated nanoparticles, which are representative of the aggregation observed in dilute nanoparticle solutions, such as that shown in **Figure 3.3.4**. Unfortunately, this effect is not observed when the nanoparticle concentration is increased to practical printing levels. In particular, the nanoparticles begin to agglomerate into macroscopic aggregates when the nanoparticle concentration is increased.

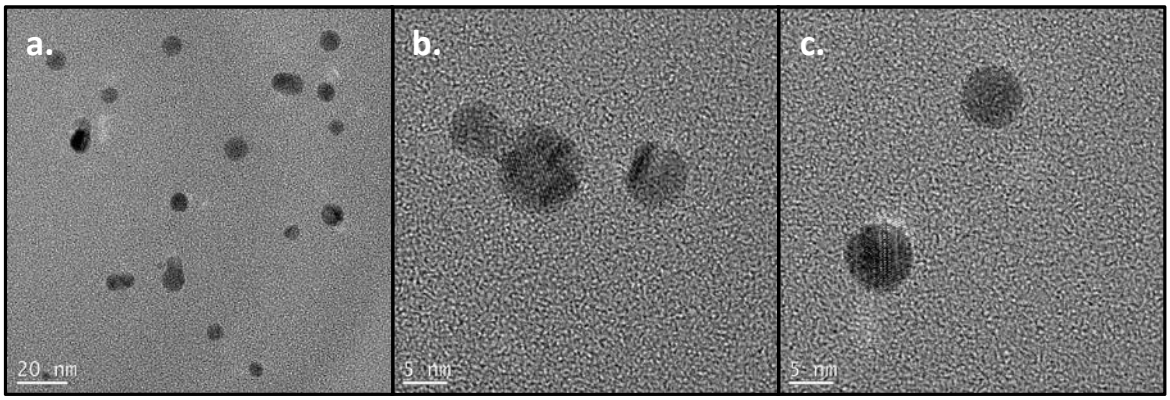

Figure 3.3.5: *a.) Transmission electron micrographs, showing a.) a typical distribution of silver nanoparticles from ink 1 b.) two weakly aggregated particles c.) two spherical particles, with diameters of approximately 5 nm, which is representative of the average particle size*

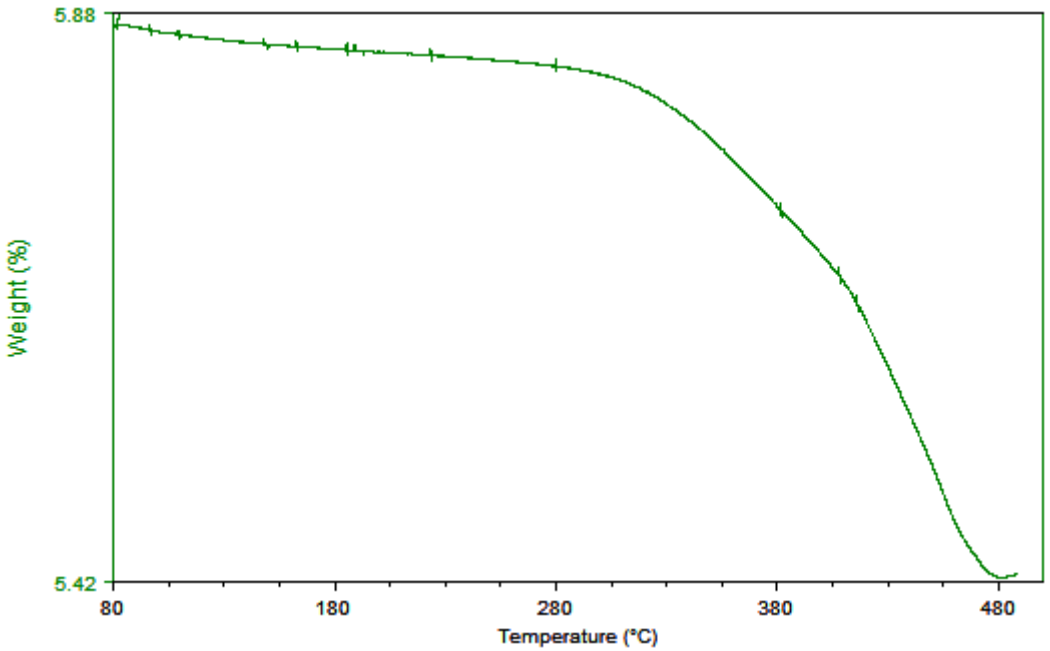

Figure 3.3.6: *Thermogravimetric analysis data of the ink synthesized in* ***Section 3.2.3***

PEDOT:PSS capped nanoparticles are significantly more soluble than nanoparticles capped with small molecules ligands. In particular, it is often necessary to add significant amounts of acetone, the weak solvent, in order to induce precipitation during centrifugation. The ink solids loading was characterized via thermogravimetric analysis, as shown in **Figures 3.3.6 and 3.3.7**.

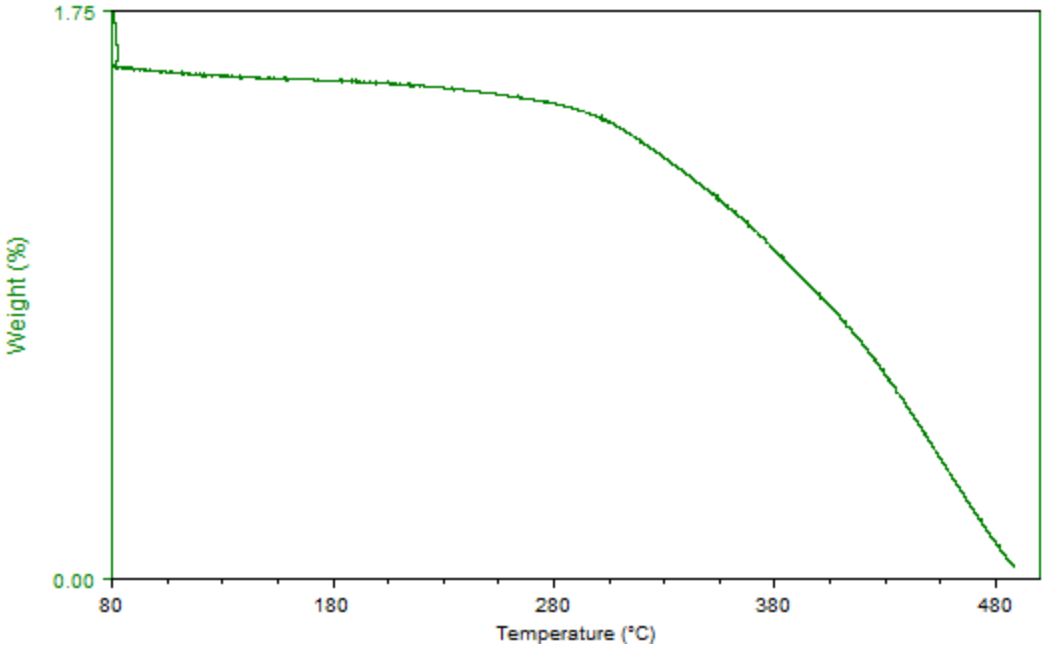

Figure 3.3.7: *Thermogravimetric analysis data of the PEDOT:PSS gelled particles*

The ink has a solids loading of 5.87 wt% , as shown in **Figure 3.3.6**. The PEDOT:PSS gelled particles begin to thermally decompose at approximately 280 °C, and have completely oxidized by the time the temperature reaches 500 °C (**Figure 3.3.7**). Based on this information, the data from **Figure 3.3.6** shows that the solid content of the ink comprises of 7.65 wt% PEDOT:PSS and 92.35 wt% silver. The ratio of PEDOT:PSS to silver dictates the ink's conductivity and conformity of the printed film. **Figures 3.3.7 and 3.3.8** below show stylus profilometer depth maps of two drop casted films, one with more PEDOT:PSS than the other.

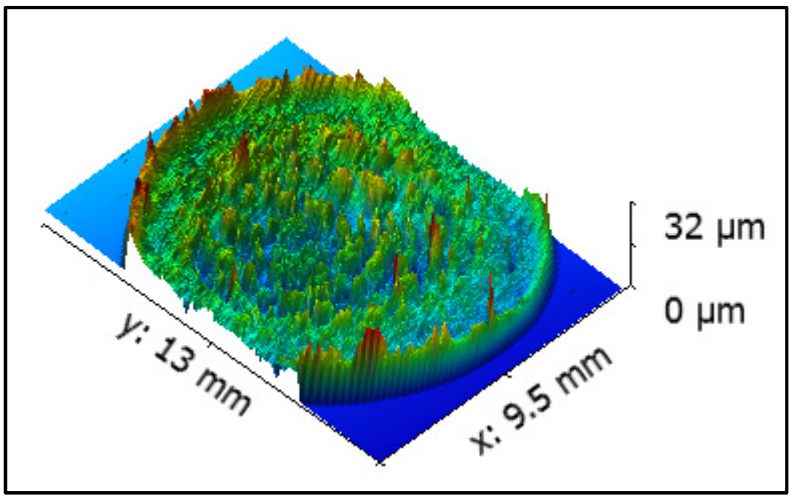

Figure 3.3.7: *Stylus profilometer depth map of a drop casted film, using a ink with minimal amounts of PEDOT:PSS*

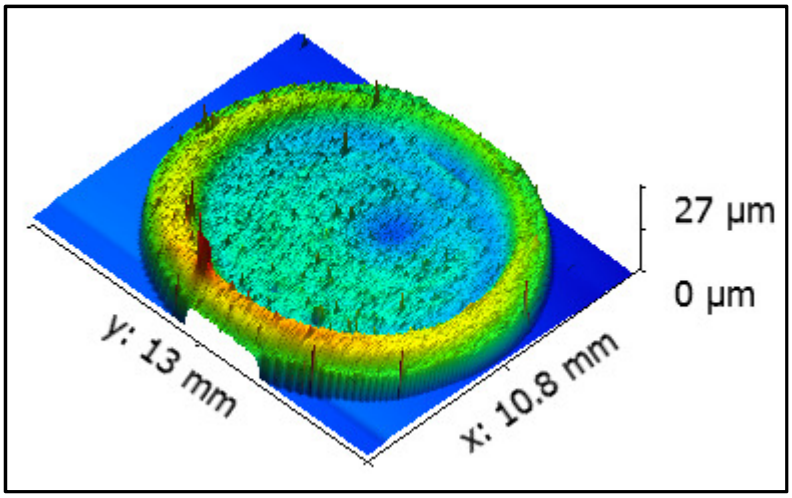

Figure 3.3.8: *Stylus profilometer depth map of a drop casted film, using the ink synthesized in* ***Section 3.2.3****, with a significantly lower surface roughness*

3.4 Conclusion

The ligand free nanoparticle synthesis procedure described in **Section 3.2.1** rapidly produces a high concentration of small nanoparticles. Unfortunately, the nanoparticles aggregate very rapidly and thus cannot be used to produce stable colloidal silver inks. The procedure described in **Section 3.2.2** explores an alternative synthesis approach, which leverages small molecule organic stabilizers to reduce agglomeration and improve ink shelf life. This synthesis technique produces high quality, sub-10 nm particles that can be printed through nanometer-

scale orifices. In addition, these nanoparticles can be synthesized at a high throughput and are ligated with capping agents that do not affect ink rheology. The optimal small molecule nanoparticle synthesis procedure was identified through many experimental iterations, based upon the resultant nanoparticle size distribution, measured via optical spectroscopy and transmission electron micrography. The nanoparticles appear to have a limited solubility in water, and tend to agglomerate when the ink is concentrated to reach nanoparticle solids loading necessary for efficient printing. While small molecule ligands are effective capping agents at low nanoparticle concentrations such as those shown in **Figure 3.3.4**, particle-particle interactions are inevitable at practical storage concentrations. As a result, these inks have a limited shelf life and tend to aggregate over the course of several weeks. In addition, it is important to note that the inks are susceptible to thermal cracking during sintering, as they lack a polymeric binder to stabilize the drop-casted films. For this reason, longer ligands are necessary to address the shelf life, nanoparticle solubility, and thermal cracking concerns. As discussed in **Section 2.4**, conventional polymeric ligands, such as poly(acrylic acid), have an adverse effect on ink rheology and electrical conductivity. The conductive ligand synthesis approach addresses the aforementioned concerns by leveraging a conductive polymer. When used as a capping agent, PEDOT:PSS improves nanoparticle solubility and reduces the surface roughness of printed films.

4. Conclusion and Future Work

Additively manufactured electronics is an emerging field of materials science and electrical engineering that has a wide range of potential applications. In particular, high performance silver nanoparticle based conductive inks have the potential to revolutionize the field of additively manufactured electronics. Additively manufactured conductive features afford numerous benefits compared to conventional electrodes. They can be printed in three dimensions,

densify printed circuit boards and interface with next-generation, additively manufactured electronic devices. At present, commercially available conductive silver inks are commonly synthesized with polymeric ligands that interfere with ink rheology, as discussed in **Section 2**. For this reason, each ink must be synthesized with a polymeric ligand that is compatible with the final printing application, thus raising the development costs of new inks. In addition, these inks must be processed at high temperatures to thermally decompose the polymeric ligands in order to reach the desired conductivity levels.

To lower ink development costs and processing temperatures, we proposed a decoupled synthesis approach, where a base ink is first synthesized with a minimal amount of ligands and the ink rheology is tailored with polymeric additives post-synthesis. We explored three different synthesis approaches, the ligand free, small molecule, and conductive ligand synthesis techniques. Ligand free nanoparticles can be synthesized at an extremely high throughput, but aggregate far too rapidly to be practically used on the commercial scale. The small molecule synthesis technique produces high quality, sub-10 nm nanoparticles that can be printed through nanometer-scale printer nozzles. Unfortunately, these nanoparticles have a limited solubility and begin to aggregate as the ink's solids loading is increased to practical printing concentrations. When printed, films tend to exhibit thermal cracking as polymeric binders are not present to stabilize the film. For this reason, we introduced a novel synthesis technique that leverages conductive polymers to improve colloidal stability, lower processing temperatures and increase electrical conductivity of silver nanoparticle based inks. In particular, our method uses PEDOT:PSS as a capping agent during nanoparticle synthesis. Preliminary results show improved ink stability and film conformity, though further testing is required to verify the ink's electrical conductivity.

In the future, I plan to further optimize the conductive ligand synthesis technique by growing larger nanoparticles at elevated temperatures. Larger nanoparticles will improve electrical conductivity by decreasing the amount of PEDOT:PSS/silver interfaces. Four-point probe tests will be used to measure electrical conductivity, and the nanoparticle size distribution will be characterized with transmission electron microscopy, dynamic light scattering, and ultraviolet-visible spectroscopy. The ink's solids loading will be characterized with thermogravimetric analysis. The film conformity and morphology will be characterized via stylus profilometry and scanning electron microscopy, respectively. If time permits, I plan to print the ink synthesized in **Section 3.2.3** on flexible substrates to characterize conductivity as a function of cyclic loading. Other research directions could include printing transparent conductive grids with the coffee ring effect or 3D structures using direct write assembly.

References:

1. Lewis, J. A.; Gratson, G. M. Direct Writing in Three Dimensions. *Mater. Today* **2004**, 7, 32–39.
2. Ahn, B. Y.; Walker, S. B.; Slimmer, S. C.; Russo, A.; Gupta, A.; Kranz, S.; Duoss, E. B.; Malkowski, T. F.; Lewis, J. A. Planar and Three-Dimensional Printing of Conductive Inks. *J. Vis. Exp.* **2011**.
3. Ahn, B. Y.; Lorang, D. J.; Lewis, J. A. Transparent Conductive Grids via Direct Writing of Silver Nanoparticle Inks. *Nanoscale* **2011**, 3, 2700–2702.
4. Sun, K.; Wei, T. S.; Ahn, B. Y.; Seo, J. Y.; Dillon, S. J.; Lewis, J. A. 3D Printing of Interdigitated Li-Ion Microbattery Architectures. *Adv. Mater.* **2013**, 25, 4539–4543.
5. Samanta, S.; Pyne, S.; Sarkar, P.; Sahoo, G. P.; Bar, H.; Bhui, D. K.; Misra, A. Synthesis of silver nanostructures of varying morphologies through seed mediated growth approach. *J. Mol. Liq.* **2010**, 170–173.
6. Kozin, E. D.; Black, N. L.; Cheng, J. T.; Cotler, M. J.; McKenna, M. J.; Lee, D. J.; Lewis, J. A.; Rosowski, J. J.; Remenschneider, A. K. Design, fabrication, and *in vitro* testing of novel three-dimensionally printed tympanic membrane grafts. *Hear. Res.* **2016**, 1–13.
7. Kolesky, D. B.; Homan, K. A.; Skylar-Scott, M. A.; Lewis, J. A. Three-dimensional bioprinting of thick vascularized tissues. *Proc. Natl. Acad. Sci.* **2016**.
8. McCracken, J. M.; Badea, A.; Kandel, M. E.; Gladman, A. S.; Wetzel, D. J.; Popescu, G.; Lewis, J. A.; Nuzzo, R. G. Programming Mechanical and Physicochemical Properties of 3D Hydrogel Cellular Microcultures via Direct Ink Writing. *Adv. Healthcare Mater.* **2016**, 1–15.
9. Sun, L.; Parker, S. T.; Syoji, D.; Wang, X.; Lewis, J. A.; Kaplan, D. L. Direct-Write Assembly of 3D Silk/Hydroxyapatite Scaffolds for Bone Co-Cultures. *Adv. Healthcare Mater.* **2012**, 729–735.
10. Adams, J. J.; Slimmer, S. C.; Lewis, J. A.; Bernhard, J. T. 3D-printed spherical dipole antenna integrated on small RF node. *Electron. Lett.* **2015**, 661–662.
11. Adams, J. J.; Duoss, E. B.; Malkowski, T. F.; Motala. M. J.; Ahn, B. Y.; Nuzzo, R. G.; Bernhard, J. T.; Lewis, J. A. Conformal Printing of Electrically Small Antennas on Three-Dimensional Surfaces. *Adv. Mater.* **2011**, 1335–1340.
12. Skylar-Scott, M. A.; Gunasekaran, S.; Lewis, J. A. Laser-assisted direct ink writing of planar and 3D metal architectures. *Proc. Natl. Acad. Sci.* **2016**.
13. Naidu, B. V. K.; Park, J. S.; Kim, S. C.; Park, S.; Lee, E.; Yoon, K.; Lee S. J.; Lee, J. W.; Gal, Y.; Jin, S. Novel hybrid polymer photovoltaics made by generation silver nanoparticles in polymer:fullerene bulk-heterojunction structures. *Sol. Energ. Mat. Sol. C.* **2008**, 397–401.
14. Mahajan, A.; Hyun, W. J.; Walker, S. B.; Lewis, J. A.; Francis, L. F.; Frisbie, C. D. High-Resolution, High-Aspect Ratio Conductive Wires Embedded in Plastic Substrates. *ACS Appl. Mater. Interfaces* **2015**, 1841–1847.

15. Walker, S. B.; Lewis, J. A. Reactive Silver Inks for Patterning High-Conductivity Features at Mild Temperatures. *J. Am. Chem. Soc.* **2012**, 1419–1421.

16. Wani, I. A.; Khatoon, S.; Ganguly, A.; Ahmed, J.; Ganguli, A. K.; Ahmad, T. Silver nanoparticles: Large scale solvothermal synthesis and optical properties. *Mater. Res. Bull.* **2010**, 1033–1038.

17. Šileikaitė, A.; Puišo, J.; Prosyčevas, I.; Tamulevičius, S. Reactive Silver Inks for Patterning High-Conductivity Features at Mild Temperatures. *J. Am. Chem. Soc.* **2009**, 21–27.

18. Baalousha, M.; Nur, Y.; Römer, I.; Tejamaya, M.; Lead, J. R. Effect of monovalent and divalent cations, anions and fulvic acid on aggregation of citrate-coated silver nanoparticles. *Sci. Total Environ.* **2013**, 119–131.

19. El Badawy, A. M.; Luxon, T. P.; Silva, R. G.; Scheckel, K. G.; Suidan, M. T.; Tolaymat, T. M. Impact of Environmental Conditions (pH, Ionic Strength, and Electrolyte Type) on the Surface Charge and Aggregation of Silver Nanoparticles Suspensions. *Environ. Sci. Technol.* **2010**, 1260–1266.

20. Tang, L.; Ye, Y.; Zhang, H.; Liao, C.; Zong, S.; Cui, Y.; Zhang, J. A series of monodisperse silver nanoparticles by a one-pot synthesis. *Nano* **2014**, 1450005.

21. Yu, J.; Kim, I.; Kim, J.; Jeongdai, J.; Larsen-Olsen, T. T.; Søndergaard, R. R.; Hösel, M.; Angmo, D.; Jørgensen, M.; Krebs, F. C. Silver front electrode grids for ITO-free all printed polymer solar cells with embedded and raised topographies, prepared by thermal imprint, flexographic and inkjet roll-to-roll processes. *Nanoscale* **2012**, 6032–6040.

22. Andersen, T. R.; Dam, H. F.; Andreasen, B.; Hösel, M.; Madsen, M. V.; Gevorgyan, S. A.; Søndergaard, R. R.; Jørgensen, M.; Krebs, F. C. A rational method for developing and testing stable flexible indium- and vacuum-free multilayer tandem polymer solar cells comprising up to twelve roll processed layers. *Sol. Energ. Mat. Sol. C.* **2014**, 735–743.

23. Georgiou, E.; Savva, A.; Neophytou, M.; Hermerschmidt, F.; Demosthenous, T.; Choulis, S. Evaporation-free Inverted organic photovoltaics using a mixture of silver nanoparticle ink formulations for solution-processed top electrodes. *Appl. Phys. Lett.* **2014**, 105, 233901.

24. Neophytou, M.; Hermerschmidt, F.; Savva, A.; Georgiou, E.; Choulis, S. A. High efficient indium tin oxide-free organic photovoltaics using inkjet-printed silver nanoparticle current collecting grids. *Appl. Phys. Lett.* **2012**, 101, 193302.

25. Franeker, J. J.; Voorthuijzen, W. P.; Gorter, H.; Hendriks, K. H.; Janssen, R. A. J.; Hadipour, A.; Andriessen, R.; Galagan, Y. All-solution-processed organic solar cells with conventional architecture. *Sol. Energ. Mat. Sol. C.* **2013**, 267–272.

26. Murali, B.; Kim, D.; Kang, J.; Kim, J. Inkjet-printing of hybrid transparent conducting electrodes for organic solar cells. *Phys. Status Solidi A* **2014**, 1801–1806.

27. Iannaccone, G.; Välimäki, M.; Jansson, E.; Sunnari, A.; Corso, G.; Bernardi, A.; Levi, M.; Turri, S.; Hast, J.; Griffini, G. Roll-to-roll compatible flexible polymer solar cells incorporating a water-based solution-processable silver back electrode with low annealing temperature. *Sol. Energ. Mat. Sol. C.* **2015**, 227–235.

28. Semaltianos, N. G.; Perrie, W.; Romani, S.; Potter, R. J.; Dearden, G.; Watkins K. G. Polymer-nanoparticle composites composed of PEDOT:PSS and nanoparticles of Ag synthesised by laser ablation. *Colloid. Polym. Sci.* **2012**, 213–220.

29. Imai, S. Enhancing electrical conductivity and electrical thermal characteristics of a PEDOT:PSS thin layer by solvent treatment and adding Ag nanoparticle solution. *Precis. Eng.* **2015**, 143–150.

30. Park, J.; Ullah, M. H.; Park, S. S.; Ha, C. Organic electroluminescent devices using quantum-size silver nanoparticles. *J. Mater. Sci. - Mater. Electron.* **2007**, S393–S397.

31. Park, E.; Kwon, O. S.; Park, S. J.; Lee, J. S.; You, S.; Jang, J. One-pot synthesis of silver nanoparticles decorated poly(3,4-ethylenedioxythiophene) nanotubes for chemical sensor application. *J. Mater. Chem.* **2012**, 1521–1526.

32. Zhang, X.; Lee, J.; Lee, G. S.; Cha, D.; Kim, M. J.; Yang, D. J.; Manohar, S. K. Chemical Synthesis of PEDOT Nanotubes. *Macromolecules* **2006**, 470–472.

33. Wang, S.; Choi, Y.; Park, H. Investigation of Ag-poly(3,4-ethylenedioxythiophene):polystyrene sulfonate nanocomposite films prepared by a one-step aqueous method. *Appl. Phys. Lett.* **2011**, 109, 124902.

34. Xiong, Z.; Dong, C.; Cai, H.; Liu, C.; Zhang, X. Composite inks of poly(3,4-ethylenedioxythiophene)/poly(styrenesulfonate)/silver nanoparticles and electric/optical properties of inkjet-printed thin films. *Mater. Chem. Phys.* **2013**, 416–422.

35. Moreno, K. J.; Moggio, I.; Arias, E.; Llarena, I.; Moya, S. E.; Ziolo, R. F.; Barrientos, H. Silver Nanoparticles Functionalized *In Situ* with the Conjugated Polymer (PEDOT:PSS). *J. Nanosci. Nanotechnol.* **2009**, 3987–3992.

36. Oldenburg S.J. Silver Nanoparticles: Properties and Applications. http://www.sigmaaldrich.com/materials-science/nanomaterials/silver-nanoparticles.html (accessed May 11, 2016).